Available online at www.synsint.com

Synthesis and Sintering

ISSN 2564-0186 (Print), **ISSN** 2564-0194 (Online)

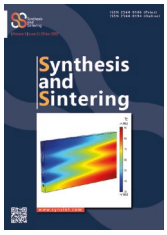

Research article

In-situ synthesized phases during the spark plasma sintering of g-C_3N_4 added TiB_2 ceramics: A thermodynamic approach

Milad Sakkaki *, Seyed Mohammad Arab

Department of Mechanical Engineering, University of Mohaghegh Ardabili, P.O. Box 179, Ardabil, Iran

ABSTRACT

In this study, in situ composite was manufactured by using TiB_2 matrix and C_3N_4 additive through spark plasma sintering. The optimum SPS parameters were considered and the process was carried out at a temperature of 1900 °C for 7 minutes by applying an external pressure of 40 MPa. The thermodynamics of possible reactions during the process were investigated. The products of the chemical reactions were identified. The complementary XRD investigations, the EDAX analysis, and SEM microscopy were used to confirm the in-situ formation of new phases. The results showed that the used carbon nitride was decomposed into its constituents, i.e., carbon and nitrogen, and the BN phase has been formed as a result of chemical reactions.

KEYWORDS

UHTC
Spark plasma sintering
SPS
Graphitic carbon nitride (g-C_3N_4)
Composite

OPEN ACCESS

1. Introduction

Thermal stability, melting temperature above 3000 °C, high resistance to thermal shocks and wear, suitable performance in corrosive environments, chemical compatibility, high electrical and thermal conductivity, and remarkable mechanical properties are the several unique characteristics of a group of materials known as ultra-high-temperature ceramics [1–5]. The UHTCs (ultra-high-temperature ceramics), which are borides, nitrides, and carbides of transition metals, have been investigated a lot for a wide range of technological applications, including electrical equipment, cutting tools, solar energy devices, aerospace applications such as leading edges of wings and nose cones of hypersonic vehicles, scramjets, and rockets [6–9]. Among UHTCs, the titanium diboride (TiB_2) which is used in this study has a 3325 °C melting point, high thermal shock resistance, high hardness and elastic modulus, good chemical neutrality, and thermal and electrical conductivity. So, it has become a very favored ceramic due to its Unique structural, physical, and thermodynamic properties [10–12]. The high melting temperature and low self-diffusion of UHTCs, which is affected by the nature of the atomic bonds of these materials (covalent bond), has made the manufacturing of fully dense parts a serious challenge. Various manufacturing methods have been developed for these materials including, hot pressing [13–14], pressureless sintering [15], laser sintering [16, 17], microwave sintering [18, 19], and spark plasma sintering [20–26]. Among the mentioned techniques, the spark plasma sintering (SPS) method has been studied and investigated a lot due to the short process time and limitation of grain growth, energy saving and cost-effectiveness, and improvement of mechanical properties [27–30]. The SPS is known as one of the most useful techniques developed for the manufacturing of ultra-high temperature ceramics. The technique is based on the simultaneous application of heat and axial pressure, based on using the Joule heating phenomenon inside the powder sample. The SPS could sinter ceramic powders in a shorter time and at a lower temperature compared to conventional methods (such as hot pressing) [31, 32]. In this method, the grain growth is significantly limited, and as a result, the final product has homogeneous finer grains, which could improve the mechanical properties [33]. SPS has been used to fabricate numerous materials such as metals and alloys, ceramics, composites, especially some amorphous materials, and structures with different grain sizes [34]. Recent studies have shown that the SPS under optimum parameters by different additives has improved different properties of TiB_2-based composites.

* Corresponding author. *E-mail address:* sakkakimilad@student.uma.ac.ir, sakkakimilad@gmail.com (M. Sakkaki)
Received 28 March 2023; Received in revised form 26 May 2023; Accepted 27 May 2023.

https://doi.org/10.53063/synsint.2023.32151

Shahedi Asl et al. [35] investigated the effects of different parameters (temperature, pressure, time, and size of secondary phase) on the grain growth and hardness of TiB_2-SiC 20 vol% composite. They have reported that the existence of SiC particles and the in-situ formation of nano-sized TiC phases limited grain growth, which resulted in a finer grain. The SPS temperature is the most prominent factor in the grain size in TiB_2-SiC composites. Based on the analysis, the sintering temperature is identified as an essential factor that has a substantial effect on hardness and grain size. Furthermore, the SPS pressure and SiC particle size played the most influential role in increasing the hardness. They got concluded that the hardness improved by increasing temperature, time, and pressure. Unlike the temperature, the holding time had no noticeable effect on the grain size and hardness.

Yin et al. [36] prepared a composite tool through a TiB_2 matrix reinforced by titanium carbide and nano-scale graphene sheets by SPS. They investigated microstructural evaluation and the effects of additives on mechanical properties and strengthening mechanisms. The results showed that the TiB_2-TiC composite with 0.1 wt% Nano-scale graphene sheets sintered at 1800 °C with a dwell time of 5 minutes, granted fully dense instances with desirable enhanced mechanical properties. The fracture toughness increased by 31.7% compared to TiB_2/TiC without graphene nanosheets. The toughness enhancement was mainly due to the bridging mechanism in the crack.

Graphitic carbon nitride (g-C_3N_4), which is often known for its catalytic applications like water treatment [37], and oxygen reduction reactions [38], recently has been found in non-catalytic applications such as an additive phase in composites [32]. Ahmadi et al. [39] suggested a new application for g-C_3N_4, by using it as a sintering aid and reinforcing phase in the ZrB_2 matrix in the SPS process. The g-C_3N_4 solved the sintering problems of ZrB_2 and improved the relative density and mechanical properties. The addition of 5 wt% of g-C_3N_4 enhanced the sintering quality and relative density of ZrB_2/g-C_3N_4 ceramics compared to the pure ZrB_2 increased from 76.5% to 99.8%.

In this research, C_3N_4 was used as an additive in the TiB_2 base composite. The possibility of in situ formation of new phases and possible reactions during the process were investigated from a thermodynamic viewpoint. The optimum parameters of the SPS were considered and the process has been carried out at 1900 °C for 7 minutes under the external pressure of 40 MPa.

2. Experimental procedure

2.1. Materials

In the present work, commercial TiB_2 powder (a product of the Chinese company, Xuzhou Hongwu Co.) with a purity of 99.9% and an average grain size of 3–8 μm used as the matrix, and g-C_3N_4 powder as the reinforcing agent.

The carbon nitride used in this research was prepared by the multiple condensation method of melamine, a product of Loba Chemie Melamine Company with a purity of 99.2%. To prepare the powder, 0.5 g of melamine was loaded into an alumina crucible and kept at a temperature of 520 °C for 240 minutes. The product then cooled down to room temperature and milled to get a fine powder.

2.2. Preparation of powder mixture

First, a sample of 10 g of TiB_2 powder and 1 g of g-C_3N_4 powder was prepared. Next, a suspension of powder was prepared in 100 cc of 96% pure ethanol. An ultrasonic bath (Daihan WUC-D10H) then was used for 30 minutes for dispersing the particles. The dispersed powder was dried by a magnetic stirrer-heater (Heidolph MR 3001 K) at 110 °C. In order to evaporate the ethanol completely, the dryer at 120 °C for 12 hours was used. Finally, the powder mixture was poured into a mortar, and after shredding, the obtained powder was passed through a sieve (mesh of 100).

2.3. SPS Process

The SPS was performed by an electrical furnace (SPS-20T-10) using graphite foils into the sample and punch interface in order to easily separate the sample and prevent conceivable reactions. Afterward, the mold was placed inside the device chamber the air inside the chamber was evacuated. The sample was sintered at a temperature of 1900 °C for 7 minutes under a pressure of 30 MPa. After sintering, the surface of the sample was polished and microstructurally studied by a field emission scanning electron microscope (Tescan Mira3). The phase analysis was carried out by an X-ray diffractometer detector (Philips PW1730). The EDS analysis also was performed to investigate the elemental composition of phases. A thermodynamic approach was used to investigate the possible reactions.

3. Results and discussion

The X-ray diffraction pattern is shown in Fig. 1. Based on the results, in the sample with 10 wt% g-C_3N_4, besides the TiB_2, the BN phase peaks were detected due to chemical reactions. The absence of C_3N_4 peaks shows the C_3N_4 is consumed completely. The thermodynamic evaluations, microstructural, and EDS analysis also confirm the BN formation and C_3N_4 consumption.

Some researchers have indicated that when TiB_2 powder exposes to the air, an oxygen-rich layer forms on the surface of the powder particles during the preparation process according to Eq. 1 [40].

$$2TiB_2(s) + 5O_2(g) \rightarrow 2TiO_2(s) + 2B_2O_3(l) \quad (1)$$

In terms of kinetics, after the formation of the first oxide layers, the oxidation rate of TiB_2 is severely limited, because the oxide layer prevents further penetration of oxygen. As the temperature increases and the sintering progresses, at 450 °C, B_2O_3 appears as a molten phase, which can increase the sintering capability of TiB_2 [41]:

$$B_2O_3(s) \rightarrow B_2O_3(l) \quad (2)$$

The C_3N_4 completely decomposed into its ingredients, i.e., carbon and nitrogen gas at a temperature of 750 °C [42]:

$$C_3N_4 \rightarrow 3C + 2N_2(g) \quad (3)$$

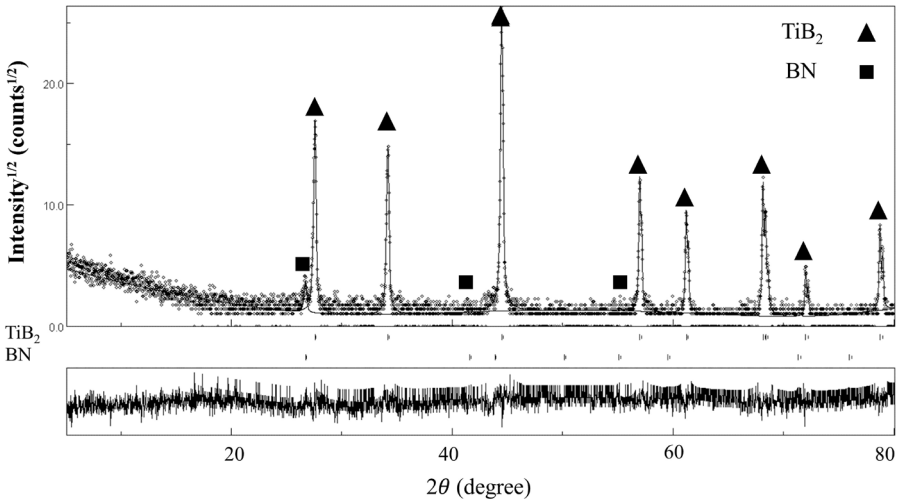

Fig. 1. XRD pattern of TiB_2-g-C_3N_4 composite.

This also proves the XRD results. The in-situ formation of BN can be caused by the reaction between the oxide components mentioned in Eq. 1 and the elements obtained from the decomposition mentioned in Eq. 3 as the following reactions:

$$B_2O_3 + 3C + N_2(g) \rightarrow 2BN + 3CO(g) \quad (4)$$

$$TiB_2 + C + N_2(g) \rightarrow TiC + 2BN \quad (5)$$

$$TiB_2 + \frac{3}{2}N_2(g) \rightarrow TiN + 2BN \quad (6)$$

$$TiO_2 + 3C \rightarrow TiC + 2CO(g) \quad (7)$$

The Gibbs free energy indicates the spontaneity of a chemical reaction. A reaction is thermodynamically more conceivable when the variation of Gibbs free energy is more negative [43].

The variation of standard Gibbs free energy for Eqs. 4–7 versus temperature is shown in Fig. 2. According to Fig. 2, the Gibbs free energy of Eqs. 5 and 6 from 100 to 1900 °C is more negative compared to other reactions, hence, these reactions are thermodynamically preferable to occur. As a result, the probability of in situ formation of BN, TiC, and TiN phases is higher. The Gibbs free energy of surface oxidation of Eqs. 4 and 7 becomes negative at 1100 °C and 1300 °C, respectively, which indicates the progress of these reactions up to the sintering temperature. i.e., 1900 °C.

It should be noted that the removal of the oxide surface of the powder particles improves the sinterability [44]. Considering the formation of BN through three of the four possible reactions, the possibility of its formation is too high. In the XRD results, besides the TiB_2, the BN phase was also detected, which was formed by situ synthesis.

The FE-SEM images of the TiB_2-g-C_3N_4 composite are shown in Fig. 3. As shown, two different regions are seen. The light gray phase is TiB_2, with some dark-colored phases scattered. Considering that C_3N_4 decomposes into its components at 750 °C, the dark areas are related to carbon.

A higher magnification FE-SEM image of the red rectangle in Fig. 3 is shown in Fig. 4. According to Fig. 4, there is a plucked area in the center of the image, which is removed and separated from the sample during the polishing process.

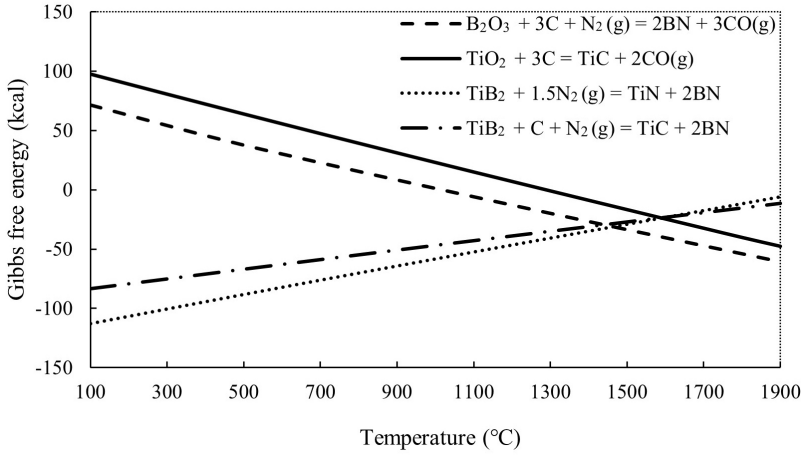

Fig. 2. The variation of standard Gibbs free energy for Eqs. 4–7 versus temperature.

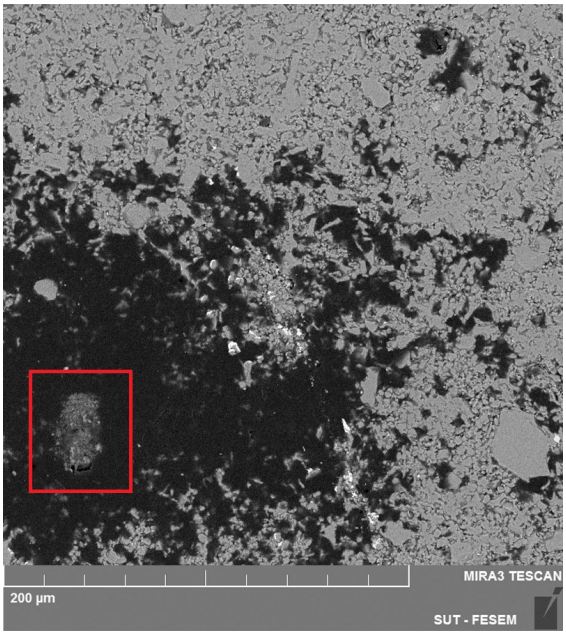

Fig. 3. The FE-SEM image of the TiB_2-g-C_3N_4 composite.

Fig. 5 illustrates the EDS results of Fig. 4. As it is evident, in the investigated section, the amount of carbon and oxygen is much higher than other elements, respectively. The areas around the plucked area of the sample, which are dark, are carbon-rich. This confirms that the C_3N_4 has been decomposed into its components of solid carbon and nitrogen gas. The EDS map of Fig. 4 is also shown in Fig. 6. According to the EDS map, the detached area of the sample was an oxidized impurity that was separated from the sample during the polishing process.

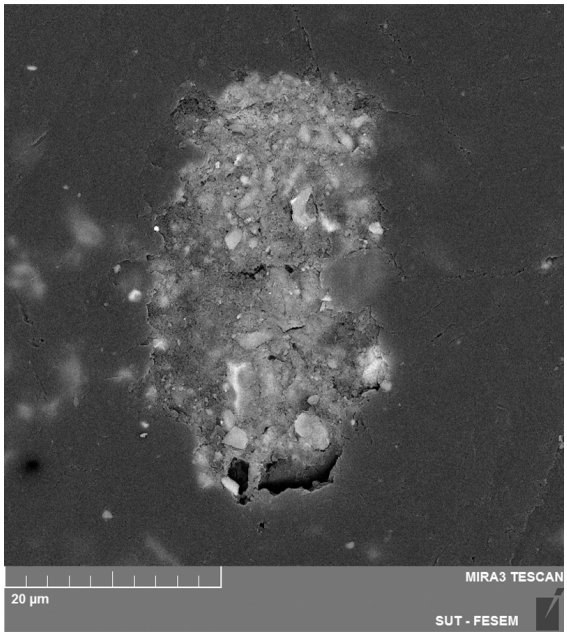

Fig. 4. A higher magnification FE-SEM image of the red rectangle in Fig. 3.

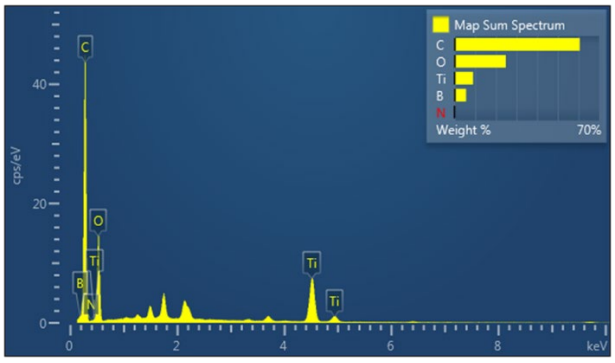

Fig. 5. EDS result of composite extracted from Fig. 4.

Furthermore, the intense concentration of carbon in the corresponding dark-colored areas in Fig. 4 is quite apparent. The presence of oxygen is obvious in the EDS map in the detached area.

An elemental x-ray map of the fracture surface of the TiB_2-g-C_3N_4 composite is presented in Fig. 7. According to the TiB_2 matrix, the accumulation of boron and titanium elements is obvious in the elemental map. The presence of nitrogen in the places where boron is aggregated confirms the in-situ formation of the BN phase.

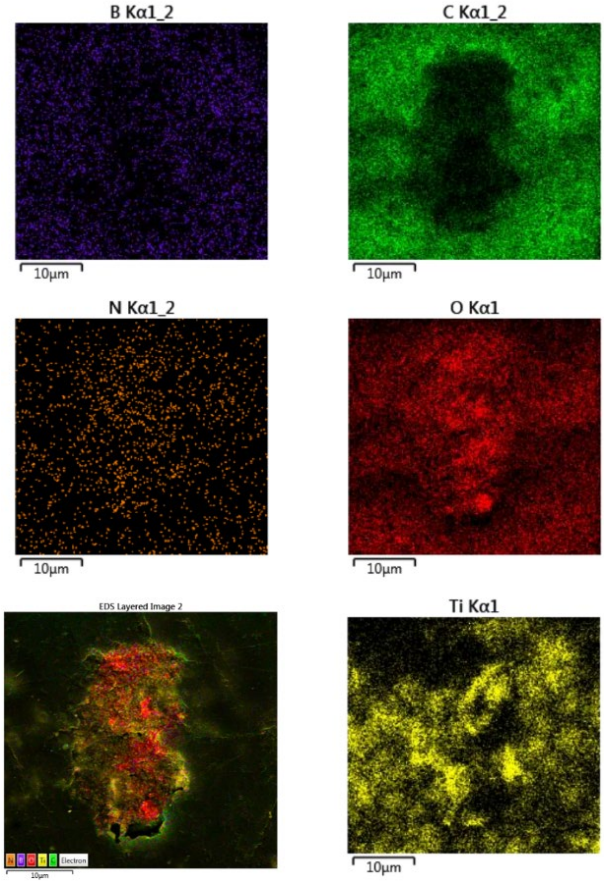

Fig. 6. EDS map of area shown in Fig. 4.

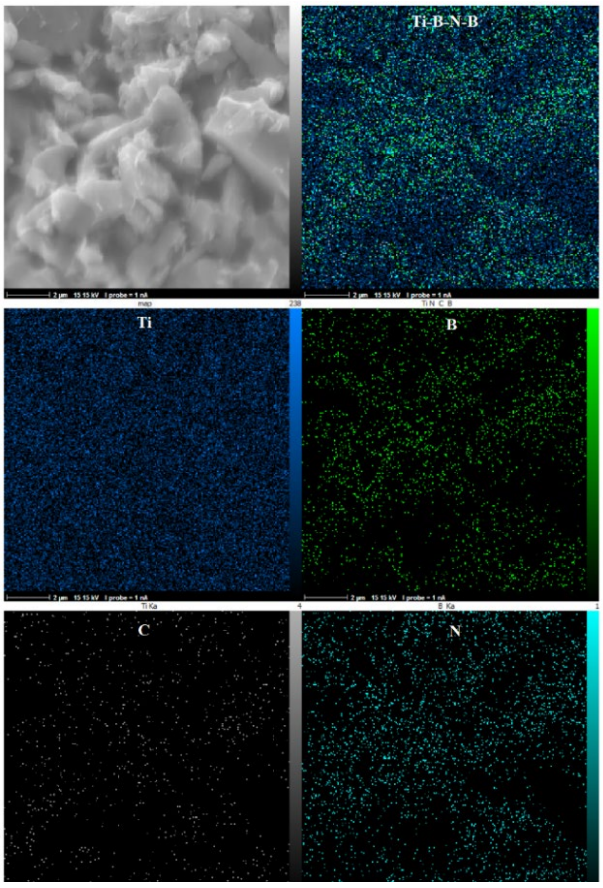

Fig. 7. FE-SEM image and EDS maps of the fracture surface of TiB_2-g-C_3N_4 composite.

4. Conclusions

In the presented work, TiB_2-based composite was manufactured using graphite carbon nitride additive by the Spark Plasma Sintering process. SPS process parameters, i.e., SPS temperature, time, and pressure optimally were considered as 1900 °C for 7 minutes by applying an external pressure of 40 MPa. In order to complete the thermodynamic analysis of the reactions, XRD tests and EDAX analysis, and microstructural investigations were carried out by the SEM microscope. The results exhibited that the used carbon nitride was decomposed into its constituents, i.e., carbon and nitrogen. Furthermore, the new BN phase was formed in situ in reaction with decomposed components of carbon nitride in the prepared composite.

CRediT authorship contribution statement

Milad Sakkaki: Conceptualization, Investigation, Writing – original draft.
Seyed Mohammad Arab: Conceptualization, Investigation, Writing – review & editing.

Data availability

The data underlying this article will be shared on reasonable request to the corresponding author.

Declaration of competing interest

The authors declare no competing interests.

Funding and acknowledgment

This article is based on the master thesis of the first author. The authors are grateful to the University of Mohaghegh Ardabili for their financial support under grant number 1401-d-14-23513.

References

[1] R.A. Cutler, Engineering Properties of Borides, ASTM Engineered Materials Handbook, ASM International, Almere. (1991).
[2] X. Jin, X. Fan, C. Lu, T. Wang, Advances in oxidation and ablation resistance of high and ultra-high temperature ceramics modified or coated carbon/carbon composites, J. Eur. Ceram. Soc. 38 (2018) 1–28. https://doi.org/10.1016/j.jeurceramsoc.2017.08.013.
[3] S.R. Levine, E.J. Opila, M.C. Halbig, J.D. Kiser, M. Singh, J.A. Salem, Evaluation of ultra-high temperature ceramics foraeropropulsion use, J. Eur. Ceram. Soc. 22 (2002) 2757–2767. https://doi.org/10.1016/S0955-2219(02)00140-1.
[4] M. Sakkaki, F. Sadegh Moghanlou, M. Vajdi, M. Shahedi Asl, M. Mohammadi, M. Shokouhimehr, Numerical simulation of heat transfer during spark plasma sintering of zirconium diboride, Ceram. Int. 46 (2020) 4998–5007. https://doi.org/10.1016/j.ceramint.2019.10.240.
[5] E. Ranjbarpour Niari, M. Vajdi, M. Sakkaki, S. Azizi, F. Sadegh Moghanlou, M. Shahedi Asl, Finite element simulation of disk-shaped HfB 2 ceramics during spark plasma sintering process, Int. J. Appl. Ceram. Technol. 19 (2022) 344–357. https://doi.org/10.1111/ijac.13886.
[6] E. Wuchina, E. Opila, M. Opeka, B. Fahrenholtz, I. Talmy, UHTCs: Ultra-High Temperature Ceramic Materials for Extreme Environment Applications, Electrochem. Soc. Interface. 16 (2007) 30–36. https://doi.org/10.1149/2.F04074IF.
[7] A. Bellosi, F. Monteverde, D. Sciti, Fast Densification of Ultra-High-Temperature Ceramics by Spark Plasma Sintering, Int. J. Appl. Ceram. Technol. 3 (2006) 32–40. https://doi.org/10.1111/j.1744-7402.2006.02060.x.
[8] S. Mohammad Bagheri, M. Vajdi, F. Sadegh Moghanlou, M. Sakkaki, M. Mohammadi, et al., Numerical modeling of heat transfer during spark plasma sintering of titanium carbide, Ceram. Int. 46 (2020) 7615–7624. https://doi.org/10.1016/j.ceramint.2019.11.262.
[9] M.J. Gasch, D.T. Ellerby, S.M. Johnson, Ultra High Temperature Ceramic Composites, Handbook of Ceramic Composites, Springer, Boston, MA. (2005) 197–224. https://doi.org/10.1007/0-387-23986-3_9.
[10] M. Saeedi Heydari, H.R. Baharvandi, Comparing the effects of different sintering methods for ceramics on the physical and mechanical properties of B4C–TiB2 nanocomposites, Int. J. Refract. Met. Hard Mater. 51 (2015) 224–232. https://doi.org/10.1016/j.ijrmhm.2015.04.003.
[11] B. Basu, G.B. Raju, A.K. Suri, Processing and properties of monolithic TiB 2 based materials, Int. Mater. Rev. 51 (2006) 352–374. https://doi.org/10.1179/174328006X102529.
[12] B.R. Golla, T. Bhandari, A. Mukhopadhyay, B. Basu, Titanium Diboride, Ultra-High Temperature Ceramics, John Wiley & Sons, Inc. (2014) 316–360. https://doi.org/10.1002/9781118700853.ch13.

[13] A. Rezaie, W.G. Fahrenholtz, G.E. Hilmas, Effect of hot pressing time and temperature on the microstructure and mechanical properties of ZrB2–SiC, J. Mater. Sci. 42 (2007) 2735–2744. https://doi.org/10.1007/s10853-006-1274-2.
[14] Y. Qin, D. Ni, B. Chen, J. Lu, F. Cai, et al., Low-temperature reactive hot-pressing of Ta 0.2 Hf 0.8 C–SiC ceramics at 1700°C, J. Am. Ceram. Soc. 106 (2023) 4390–4398. https://doi.org/10.1111/jace.19090.
[15] F. Kuang, Y. Pan, J. Zhang, X. Wu, X. Lu, Microstructure, mechanical properties, and strengthening mechanism of high performance Ti-6Al-4V alloy by pressureless sintering and hot extrusion, J. Alloys Compd. 951 (2023) 169990. https://doi.org/10.1016/j.jallcom.2023.169990.
[16] Z. Wu, C. Shi, A. Chen, Y. Li, S. Chen, et al., Large-Scale, Abrasion-Resistant, and Solvent-Free Superhydrophobic Objects Fabricated by a Selective Laser Sintering 3D Printing Strategy, Adv. Sci. 10 (2023) 2207183. https://doi.org/10.1002/advs.202207183.
[17] A.B. Peters, C. Wang, D. Zhang, A. Hernandez, D.C. Nagle, et al., Reactive laser synthesis of ultra-high-temperature ceramics HfC, ZrC, TiC, HfN, ZrN, and TiN for additive manufacturing, Ceram. Int. 49 (2023) 11204–11229. https://doi.org/10.1016/j.ceramint.2022.11.319.
[18] A.S. Lemine, O. Fayyaz, R.A. Shakoor, Z.Ahmad, J. Bhadra, N.J. Al-Thani, Effect of cold and hot compactions on corrosion behavior of p- and n-type bismuth telluride-based alloys developed through microwave sintering process, J. Alloys Compd. 939 (2023) 168763. https://doi.org/10.1016/j.jallcom.2023.168763.
[19] N. Vasudevan, N.N. Ahamed, B. Pavithra, A. Aravindhan, B.P. Shanmugavel, Effect of Ni addition on the densification of TiC: A comparative study of conventional and microwave sintering, Int. J. Refract. Met. Hard Mater. 87 (2020) 105165. https://doi.org/10.1016/j.ijrmhm.2019.105165.
[20] J.K. Sonber, T.S.R. Murthy, C. Subramanian, R.C. Hubli, A.K. Suri, Processing Methods for Ultra High Temperature Ceramics, MAX Phases and Ultra-High Temperature Ceramics for Extreme Environments, IGI Global. (2013) 180–202. https://doi.org/10.4018/978-1-4666-4066-5.ch006.
[21] Y. Le Godec, S. Le Floch, Recent Developments of High-Pressure Spark Plasma Sintering: An Overview of Current Applications, Challenges and Future Directions, Materials (Basel). 16 (2023) 997. https://doi.org/10.3390/ma16030997.
[22] B. Nayebi, M. Shahedi Asl, M.G. Kakroudi, I. Farahbakhsh, M. Shokouhimehr, Interfacial phenomena and formation of nano-particles in porous ZrB2 –40 vol% B 4 C UHTC, Ceram. Int. 42 (2016) 17009–17015. https://doi.org/10.1016/j.ceramint.2016.07.208.
[23] D. Agrawal, Microwave Sintering of Ceramics, Composites and Metallic Materials, and Melting of Glasses, Trans. Indian Ceram. Soc. 65 (2006) 129–144. https://doi.org/10.1080/0371750X.2006.11012292.
[24] C.-N. Sun, M.C. Gupta, Laser Sintering of ZrB2, J. Am. Ceram. Soc. 91 (2008) 1729–1731. https://doi.org/10.1111/j.1551-2916.2008.02369.x.
[25] Z. Ahmadi, B. Nayebi, M. Shahedi Asl, M. Ghassemi Kakroudi, Fractographical characterization of hot pressed and pressureless sintered AlN-doped ZrB2–SiC composites, Mater. Charact. 110 (2015) 77–85. https://doi.org/10.1016/j.matchar.2015.10.016.
[26] M. Tokita, Trends on advanced SPS spark plasma sintering, J. Soc. Powder Technol. Jpn. 30 (1993) 790–804. https://doi.org/10.4164/sptj.30.11_790.
[27] P. Cavaliere, B. Sadeghi, A. Shabani, Spark Plasma Sintering: Process Fundamentals, in Spark Plasma Sintering of Materials, Cham: Springer International Publishing. (2019) 3–20. https://doi.org/10.1007/978.
[28] Y. Achenani, M. Saâdaoui, A. Cheddadi, G. Bonnefont, G. Fantozzi, Finite element modeling of spark plasma sintering: Application to the reduction of temperature inhomogeneities, case of alumina, Mater. Des. 116 (2017) 504–514. https://doi.org/10.1016/j.matdes.2016.12.054.
[29] D. Salamon, K. Maca, Z. Shen, Rapid sintering of crack-free zirconia ceramics by pressure-less spark plasma sintering, Scr. Mater. 66 (2012) 899–902. https://doi.org/10.1016/j.scriptamat.2012.02.013.
[30] J.P. Kelly, O.A. Graeve, Spark Plasma Sintering as an Approach to Manufacture Bulk Materials: Feasibility and Cost Savings, JOM. 67 (2015) 29–33. https://doi.org/10.1007/s11837-014-1202-x.
[31] R.S. Dobedoe, G.D. West, M.H. Lewis, Spark plasma sintering of ceramics: understanding temperature distribution enables more realistic comparison with conventional processing, Adv. Appl. Ceram. 104 (2005) 110–116. https://doi.org/10.1179/174367605X16662.
[32] M. Sakkaki, S.M. Arab, Non-catalytic applications of g-C3N4: A brief review, Synth. Sinter. 2 (2022) 176–180. https://doi.org/10.53063/synsint.2022.24126.
[33] Z.A. Munir, U. Anselmi-Tamburini, M. Ohyanagi, The effect of electric field and pressure on the synthesis and consolidation of materials: A review of the spark plasma sintering method, J. Mater. Sci. 41 (2006) 763–777. https://doi.org/10.1007/s10853-006-6555-2.
[34] C. Shearwood, Y.Q. Fu, L. Yu, K.A. Khor, Spark plasma sintering of TiNi nano-powder, Scr. Mater. 52 (2005) 455–460. https://doi.org/10.1016/j.scriptamat.2004.11.010.
[35] M. Shahedi Asl, Z. Ahmadi, S. Parvizi, Z. Balak, I. Farahbakhsh, Contribution of SiC particle size and spark plasma sintering conditions on grain growth and hardness of TiB2 composites, Ceram. Int. 43 (2017) 13924–13931. https://doi.org/10.1016/j.ceramint.2017.07.121.
[36] Z. Yin, J. Yuan, W. Xu, K. Liu, S. Yan, Graphene nanosheets toughened TiB2-based ceramic tool material by spark plasma sintering, Ceram. Int. 44 (2018) 8977–8982. https://doi.org/10.1016/j.ceramint.2018.02.098.
[37] Y. Wang, X. Wang, M. Antonietti, Polymeric Graphitic Carbon Nitride as a Heterogeneous Organocatalyst: From Photochemistry to Multipurpose Catalysis to Sustainable Chemistry, Angew. Chem. Int. Ed. 51 (2012) 68–89. https://doi.org/10.1002/anie.201101182.
[38] H.-S. Zhai, L. Cao, X.-H. Xia, Synthesis of graphitic carbon nitride through pyrolysis of melamine and its electrocatalysis for oxygen reduction reaction, Chin. Chem. Lett. 24 (2013) 103–106. https://doi.org/10.1016/j.cclet.2013.01.030.
[39] Z. Ahmadi, M. Zakeri, A. Habibi-Yangjeh, M. Shahedi Asl, A novel ZrB2–C3N4 composite with improved mechanical properties, Ceram. Int. 45 (2019) 21512–21519. https://doi.org/10.1016/j.ceramint.2019.07.144.
[40] S. Baik, P.F. Becher, Effect of Oxygen Contamination on Densification of TiB2, J. Am. Ceram. Soc. 70 (1987) 527–530. https://doi.org/10.1111/j.1151-2916.1987.tb05699.x.
[41] V.-H. Nguyen, S.A. Delbari, Z. Ahmadi, A. Sabahi Namini, Q.V. Le, et al., Effects of discrete and simultaneous addition of SiC and Si3N4 on microstructural development of TiB2 ceramics, Ceram. Int. 47 (2021) 3520–3528. https://doi.org/10.1016/j.ceramint.2020.09.196.
[42] A. Gashi, Preparation of g-C3N4 based material and analytical characterizations for environmental applications, Material chemistry. Université de Haute Alsace - Mulhouse; The University of Ostrava. (2022).
[43] M.E. Argun, S. Dursun, C. Ozdemir, M. Karatas, Heavy metal adsorption by modified oak sawdust: Thermodynamics and kinetics, J. Hazard. Mater. 141 (2007) 77–85. https://doi.org/10.1016/j.jhazmat.2006.06.095.
[44] F. Monteverde, S. Guicciardi, A. Bellosi, Advances in microstructure and mechanical properties of zirconium diboride based ceramics, Mater. Sci. Eng. A. 346 (2003) 310–319. https://doi.org/10.1016/S0921-5093(02)00520-8.